Zeitschrift für Physikalische Chemie, Bd. 185, S. 51 – 68 (1994)

Magnesium Insertion in Vanadium Oxides: A Structural Study

By Petr Novák

Paul Scherrer Institute, Electrochemistry Section, CH-5232 Villigen PSI, Switzerland

Valery Shklover and Reinhard Nesper

Institute of Crystallography and Petrography, and Laboratory for Inorganic Chemistry, ETH-Zentrum, CH-8092 Zürich, Switzerland

Dedicated to Professor Dr. Wolf Vielstich on the occasion of his 70th birthday

(Received July 7, 1993; accepted August 30, 1993)

Magnesium battery / Vanadium oxides / Mg^{2+} ion insertion / X-ray diffraction / Electrochemistry

X-ray powder diffraction patterns of V_2O_5-related electrode materials [V_2O_5, NaV_3O_8 and $Mg(V_3O_8)_2$] as well as of poly(tetrafluoroethylene)-bonded composite electrodes, containing chemically and electrochemically inserted Mg^{2+}, were analysed before and after Mg^{2+} insertion. Transmission electron microscopy and both wavelength and energy dispersive electron probe microanalysis were applied for the determination of the composition and structure of different types of microparticles found in the electrode mass.

Röntgen-Pulverdiffraktogramme einiger V_2O_5-verwandten Mg^{2+}-einlagernden Elektrodenmaterialien [V_2O_5, NaV_3O_8 und $Mg(V_3O_8)_2$] sowie der Polytetrafluoroethylen-haltigen Verbundelektroden wurden vor und nach der chemischen sowie elektrochemischen Einlagerung von Mg^{2+} ausgewertet. Transmissions-Elektronenmikroskopie sowie wellenlängen- und energieaufgelöste Elektronen-Mikroprobenanalyse wurden für die Bestimmung von Zusammensetzung und Struktur der in der Elektrodenmasse gefundenen verschiedenen Mikroteilchen eingesetzt.

1. Introduction

High energy density rechargeable ion transfer batteries are currently under development in many laboratories. They consist of an alkali metal negative electrode, an aprotic (nonaqueous) electrolyte, and a positive insertion electrode. The merit of this concept is that the same number of cations

generated at one of the electrodes is at the same time consumed at the opposite electrode. Thus, in contrast to customary batteries there is no need for comparatively large electrolyte volumes.

Due to its natural abundance, low equivalent weight, and low price, metallic magnesium might be an alternative to lithium or sodium in a future ion transfer battery [1 – 4]. Unfortunately, the magnesium electrochemistry at ambient temperatures is far from being well understood, and only few compounds containing inserted magnesium ions have been mentioned in the literature [1 – 14].

We regard V_2O_5 and other related vanadium oxides as promising electroactive materials for the positive insertion electrode of a secondary Mg-battery [3, 4]. Mg^{2+} ions can be inserted in the oxide chemically or electrochemically. An overall scheme for the electrochemical reaction can be written as

$$V_2O_5 + x\,Mg^{2+} + 2x\,e^- \Leftrightarrow Mg_xV_2O_5\,.$$

Electrochemical tests have shown that the insertion reactions are fairly reversible. The amount of Mg^{2+} inserted in V_2O_5 depends on the nature of the electrolyte, on the ratio between the amounts of H_2O and Mg^{2+} in the solution as well as on the absolute amount of H_2O in the electrolyte [3]. The highest coulombic capacities [1], about 200 Ah/kg, were reached on V_2O_5 (and V_6O_{13}) in acetonitrile solution containing 1 *M* $Mg(ClO_4)_2$ + 1 *M* H_2O [3, 15]. The amount of Mg^{2+} inserted in V_2O_5 decreases with the decreasing amount of H_2O in the solution and approaches about 20 Ah/kg in fairly dry electrolytes [3].

In order to facilitate the Mg^{2+} insertion in the interlayer space of the oxide, we attempted to increase the distance between the V_2O_5 layers by introducing metal ions in the V_2O_5 lattice, forming, thus, vanadium bronzes. Indeed, several vanadium bronzes such as NaV_3O_8 and $Mg(V_3O_8)_2$ show promising coulombic capacities of up to 110 Ah/kg in rigorously dry electrolytes [4].

Obviously, variations in the crystal structure of the insertion materials influence their ability to accommodate Mg^{2+} or other metal ions. The present work attempts to determine the structures of the Mg^{2+}-inserted V_2O_5 as well as of the vanadium bronzes (which are both poorly crystalline). Efforts have been made to correlate the results of the crystallographic structural analysis of the vanadium bronzes with their electrochemical behaviour, with the aim of gaining information necessary for the future design and optimisation of the synthesis of bronzes with higher coulombic capacity.

[1] Coulombic capacity is defined as charge stored in 1 kg of the oxide and corresponds with the amount of Mg^{2+} inserted in the oxide.

Table 1. Scheme of preparation of Mg-inserted vanadium oxides*.

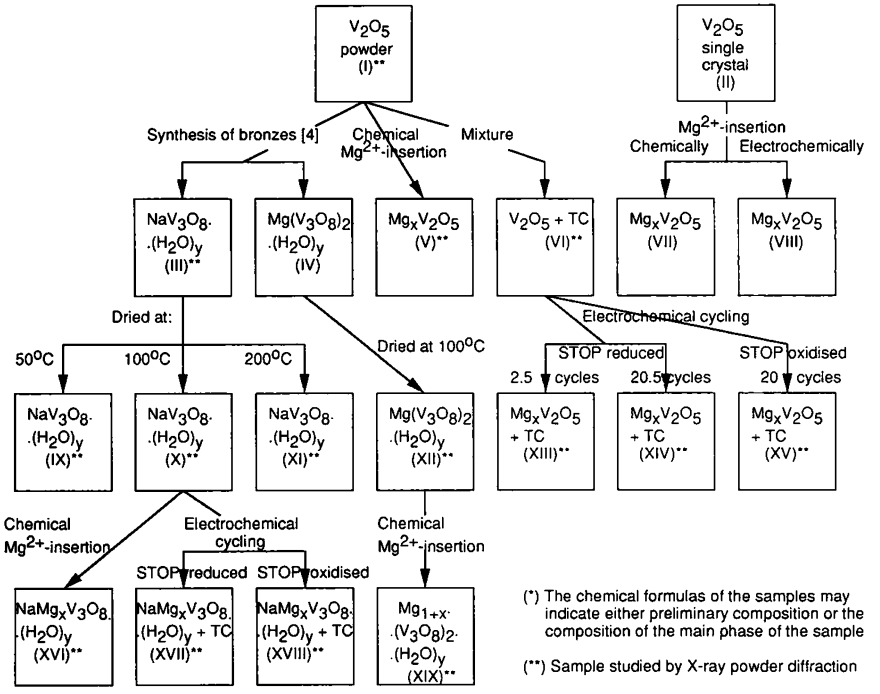

2. Experimental

2.1. Materials

As received V_2O_5 powder (**I**, Aldrich, 99.6+ %) and V_2O_5 single crystals[2] (**II**) were used as starting materials for the experiments (Table 1). The bronzes, NaV_3O_8 and $Mg(V_3O_8)_2$ were prepared as in [4]: an aqueous solution of NaOH, or an aqueous suspension of MgO, was stirred with a stoichiometric amount of V_2O_5 (**I**) at $\sim 50°C$ overnight. The orange-yellow colour of V_2O_5 turned gradually to red-brown under slow precipitation of the hydrated bronze, $NaV_3O_8(H_2O)_y$ (**III**) or $Mg(V_3O_8)_2(H_2O)_y$ (**IV**). The latter was filtered, washed with H_2O, and vacuum-dried at room temperature for several days. After a mild grinding, the hydrated bronze was further dried under dynamic vacuum at 50, 100, or 200°C overnight (**IX–XII**, Table 1). Note, the formula $(H_2O)_y$ denotes an unknown, variable amount of bound water, including $y = 0$.

[2] The V_2O_5 single crystals, a gift of Dr. K. Kato of the National Institute for Research in Inorganic Materials, Tsukuba, Japan, were prepared by Y. Uchida and E. Bannai from reagent grade V_2O_5 of 99.99% purity using the floating-zone technique in an image furnace [16]. Detailed results of investigations of Mg^{2+}-inserted single crystals will be reported in a forthcoming paper.

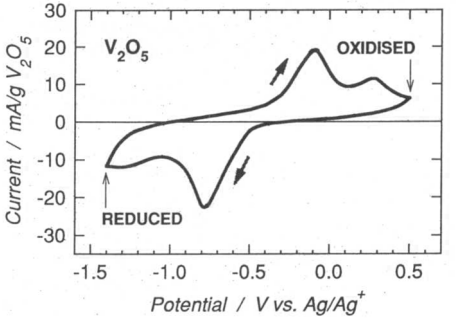

Fig. 1. Cyclic voltammogram (first cycle at 0.02 mV/s) in the 1 *M* $Mg(ClO_4)_2$ + 1 *M* H_2O/AN electrolyte of a V_2O_5 electrode containing 50 wt.% teflonised carbon (**VI**).

2.2. Magnesium insertion

The compounds V_2O_5 (**I, II**), NaV_3O_8 (**IX–XI**) and $Mg(V_3O_8)_2$ (**XII**) were screened for their ability to insert (excess) Mg^{2+} via chemical and electrochemical tests. Chemical insertion experiments involved placing either about 0.5 g of a powdery material or a V_2O_5 single crystal (**II**) in contact with excess 1 *M* dibutylmagnesium solution in heptane (Aldrich) under an Ar atmosphere, and allowing them to react under occasional stirring at room temperature for two months. The materials were then rinsed with heptane several times, dried, and examined for structural changes via X-ray diffraction.

The electrochemical insertion of Mg^{2+} in V_2O_5, NaV_3O_8 and $Mg(V_3O_8)_2$ was investigated using cyclic voltammetry at very slow potential sweep rates. To give the working electrodes sufficient electronic conductivity and mechanical stability, each of the electroactive materials was dry-mixed with an equal part of TC (Teflonised Carbon: 25 wt.% PTFE + 75 wt.% acetylene black), and the mixture was spread by pressing on a current collector. To avoid oxygen and moisture contamination, all succeeding manipulations and measurements described below were performed either in an Ar-filled glove box in which the H_2O and O_2 levels were not permitted to exceed 5 ppm, or in hermetically sealed cells assembled in the glove box.

Electrochemical experiments were performed in two kinds of electrolytes: (i) at room temperature in acetonitrile (AN) solutions containing 1 *M* $Mg(ClO_4)_2$ and various amounts (0.02 *M* – 2.5 *M*) of H_2O, and (ii) at 80°C in room temperature molten salts. The salt melt contained 3 wt.% $MgCl_2$, 56 wt.% $AlCl_3$ and 41 wt.% 1-ethyl-3-methylimidazolium chloride (EMIC). The experimental details have been described elsewhere [3, 4]. Conventional glass cells with a free-hanging working electrode, as well as cells with working and counter electrodes pressed together with a spring were employed. (With the latter cells, better electrochemical performance at higher sweep rates, due to better electrical contact of the electroactive particles to the current collector, was observed.) The working electrodes had geometrical areas of 1.3 – 1.5 cm^2 and contained 10 – 20 mg of electroactive material. For the sake of comparison, the currents were normalised by the mass of the electroactive material. A magnesium counterelectrode and an Ag/Ag^+ reference electrode were used in AN based solutions. In the salt melt, metallic aluminium served as the counterelectrode against which the potentials were also measured.

Electrochemically treated samples for X-ray powder diffraction measurements were prepared as follows: The working electrode was voltammetrically cycled, starting with a reduction sweep from the open circuit potential. Then, it was stabilised in the oxidised or reduced state at the appropriate potential (Fig. 1) overnight, removed from the cell,

washed in dry deoxygenated acetonitrile overnight, and dried in the glove box atmosphere for several days. The electrode mass scraped from the current collector was loaded in a glass capillary which was sealed afterwards.

Electrochemical magnesium insertion experiments were performed also with V_2O_5 single crystals. The crystals were contacted by pressing them against a glassy carbon current collector, using the spring-loaded electrochemical cell described above. The electrolyte was 1 *M* $Mg(ClO_4)_2$ + 0.9 *M* H_2O in AN. In a typical experiment, the potential was sweeped at 0.5 μV/s from its open circuit value to −1.4 V (vs. Ag/Ag^+). Then, the single crystal was reduced at −1.4 V for 5 weeks. During this procedure, the orange-yellow colour of the V_2O_5 turned dark. The reduced crystal was washed with dry deoxygenated AN, dried in the glove box atmosphere, and analysed afterwards.

2.3. Structural investigations

X-ray powder diffraction patterns of samples **I**, **III**, **V**, **VI** and **IX**−**XIX**, sealed under an inert atmosphere in glass capillaries, were recorded using a STOE automatic powder diffractometer (CuK_α radiation, Ge monochromator, small linear position sensitive detector, data collection in Debye mode, 150 steps within the 2Θ interval of 5−80°, 1000 sec per step). The patterns of the samples were indexed with the TREOR and LATCON programs.

A single crystal four-circle Nicolet diffractometer as well as a light microscope were used to study the electrochemically treated V_2O_5 sample **VIII**.

Transmission electron microscopy (TEM) studies of the samples **XIII** and **XIV** were performed on a Philips SM 30 ST transmission electron microscope equipped with a detector for energy dispersive X-ray spectrometry (EDX) and a STEM attachment, as well as with a Philips 500 scanning microscope with an EDX attachment.

Wavelength dispersive electron probe microanalysis (EPMA) [17] was applied for the determination of the Mg content in **V**, **XII**, **XVI** and **XIX** using a Cameca SX50 equipped with five spectrometers (accelerating voltage 20 kV, beam current 20 μA).

Solid state NMR spectra of the sample **III** were recorded with a Brucker AMX400 spectrometer equipped with a Wide-Bore-Magnet (B_o = 9.4 Tesla) and a high-speed double-bearing MAS-probe.

3. Results and discussion

3.1. Hydrated sodium vanadium bronzes III, IX, X and XI

To avoid a possible reaction of metallic magnesium with water, fairly dry electrolytes are preferred in a Mg battery. Because our preliminary electrochemical experiments have shown that the coulombic capacity of pure V_2O_5 significantly decreases with the decreasing amount of water in the electrolyte [3], vanadium bronzes of the LiV_3O_8 type were synthesised and tested for Mg^{2+} insertion. In contrast to the V_2O_5 case, the bronzes allow an electrochemical insertion of Mg^{2+} from a rigorously dry environment. As reported in [4], coulombic capacities of up to 110 Ah/kg were reached for the best samples of NaV_3O_8.

It follows from the comparison of coulombic capacities of the bronzes **IX**−**XI** dried at different temperatures that NaV_3O_8 dried at 200°C is

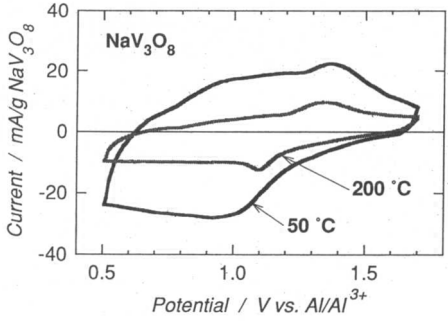

Fig. 2. Cyclic voltammograms (third cycles at 0.05 mV/s) in the $MgCl_2/AlCl_3$/EMIC salt melt of $NaV_3O_8(H_2O)_y$ dried at 50°C (**IX**) and 200°C (**XI**). The electrode contained 50 wt.% teflonised carbon.

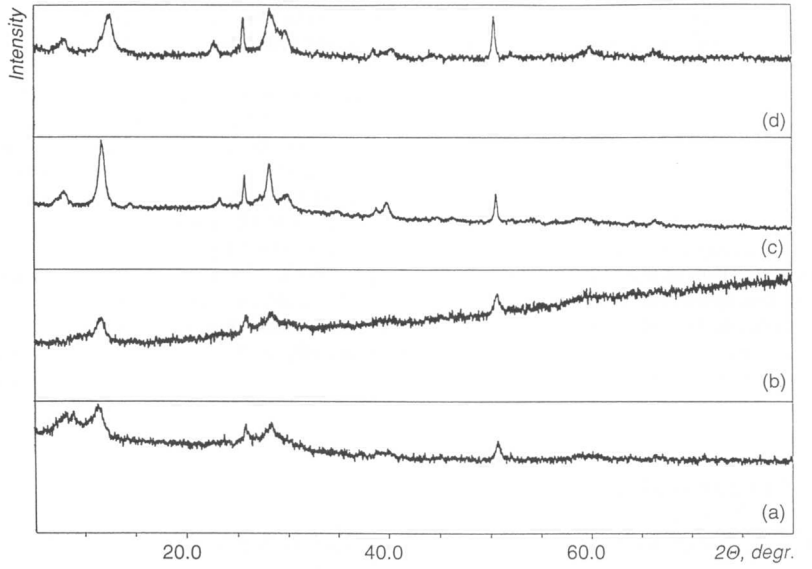

Fig. 3. X-ray powder diffraction patterns of (a) the bronze $NaV_3O_8(H_2O)_y$ (**III**), and of the products of its drying at (b) 50°C (**IX**), (c) 100°C (**X**) and (d) 200°C (**XI**).

electrochemically much less active than the bronzes dried at $\leq$100°C. (There is no significant variance between the coulombic capacities of the 50 and 100°C samples.) This effect is illustrated in Fig. 2.

X-ray diffraction patterns of the (poorly crystalline) bronze $NaV_3O_8(H_2O)_y$ (**III**) and the products **IX**, **X** and **XI** of drying of **III** at 50, 100 and 200°C are similar. The patterns have four common basic peaks (found at 2Θ = 11.31°, 25.84°, 28.31° and 50.73° for **III**) (Fig. 3,

Table 2. Positions (2 Θ, degree) and intensities (I) of the peaks on the X-ray diffraction patterns of $NaV_3O_8(H_2O)_y$ (**III**) and the products of drying of **III** at 50°C (**IX**), 100°C (**X**), and 200°C (**XI**).

III		**IX**		**X**		**XI**		
2 Θ	I	2 Θ	I	2 Θ	I	2 Θ	I	*hkl**
				7.30	13			
8.13	40			8.05	25	8.03	35	100
8.90	52			8.24	20	8.23	35	
				11.42	44			
11.31	100	11.61	100	11.78	100	11.72	40	001
						12.55	88	
				14.64	10			200
						22.88	36	
				23.32	16			
25.84	79	25.87	85	25.82	51	25.73	82	110
				27.30	13			
28.31	76	28.34	67	28.30	58	28.28	87	
						28.52	74	111
						28.88	53	
				30.12	20	30.15	32	−211
				34.86	14			−103
				38.90	19	38.68	27	−410
				39.85	28			−303
				40.04	25			
						40.29	27	
						40.60	26	
50.73	50	50.70	98	50.66	47	50.50	100	204
						60.12	30	
						66.34	27	−323
				66.47	10			305

* Reflections indexed with the unit cell of barnesite (a = 12.17 Å, b = 3.602 Å, c = 7.78 Å, β = 95°2′, V = 342.0 Å^3 [18]).

Table 2). The shift to larger 2 Θ values in the series **III** → **IX** → **X** → **XI** and the splitting (samples **X** and **XI**) of the first peak (at 2 Θ = 11.31° in **III**), and the approximate conservation of the positions of the three other basic peaks are worthy of attention. The single crystal data published for $NaV_3O_8(H_2O)_{1.5}$ [18] (existing in nature as the mineral barnesite) were used for the indexing of the patterns of **III** and **IX**−**XI**. Minor changes of the two unit cell parameters b and c, and a large successive decrease of the parameter a accompanied with a successive decrease of the unit cell volume with the increasing drying temperature (transition **III** → **IX** → **X** → **XI**) were observed. (Note that a lattice constant variation within one phase was observed also for the ε-phase of $Li_xV_2O_5$ bronzes [19].)

One may suggest a layered character of the crystal structure of the phases **III** and **IX**−**XI**, a conservation of the structure within the layers,

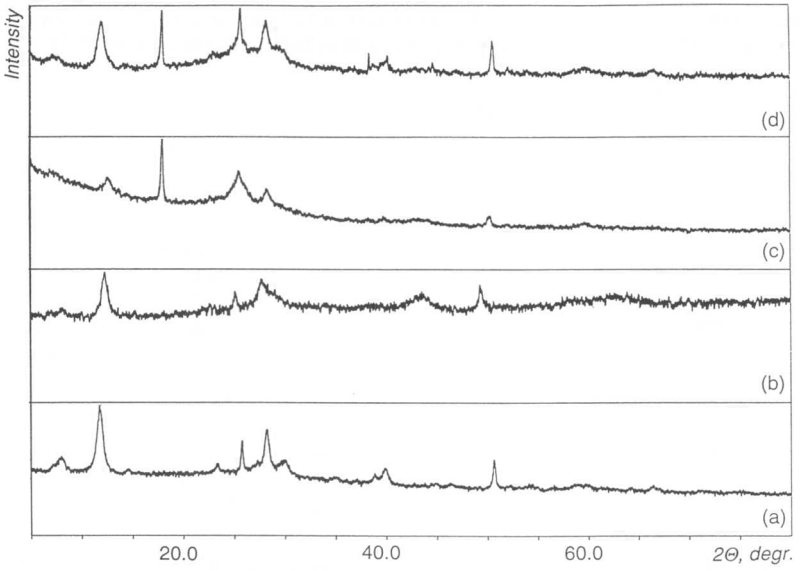

Fig. 4. X-ray powder diffraction patterns of (a) the bronze $NaV_3O_8(H_2O)_y$ dried at 100°C (**X**), and the products of (b) chemical (**XVI**) and (c, d) electrochemical (**XVII**, c and **XVIII**, d) Mg^{2+} insertion in **X**.

and a decrease of the interlayer separation with water removal. The splitting of the first basic peak of **X** and **XI** may indicate a coexistence of two phases with different water content in the samples **X** and **XI** (**Xa** and **Xb**, **XIa** and **XIb**). Thus, the drying process probably proceeds in distinct steps, as, e.g., reported for the removal of excess water from the solid gel $V_2O_5 \cdot y\ H_2O$ [20].

A similar abrupt change of the unit cell parameters, occurring during a water removal in the course of heating as observed for **III** and **IX**–**XI**, was reported earlier for the transition of hydrated sodium metavanadate: $NaVO_3(H_2O)_2 \rightarrow$ (transition phase) $\rightarrow \beta$-$NaVO_3$ [21]. The closeness of the unit cell sizes of the studied hydrated sodium vanadium bronzes and the cited metavanadates is remarkable, but a ^{51}V solid state NMR study of the sample **III** clearly indicated an octahedral coordination, and not the tetrahedral coordination of vanadium atoms characteristic for metavanadates ($\delta_{iso} = -533 \pm 10$ ppm, $\delta = 657 \pm 10$ ppm, $\delta_1 = \delta_2 = -290 \pm 10$ ppm, $\delta_3 = -947 \pm 10$ ppm; for the interpretation of the solid state NMR data on vanadium compounds see [22]).

Combining the electrochemical and structural results, it seems to be reasonable to suggest that the hydrated bronze, $NaV_3O_8(H_2O)_{1.5}$, is electrochemically the most active constituent of the obtained Na-bronzes. Pronounced structural changes occur during the drying of this bronze above

Table 3. Positions (2Θ, degree) and intensities (I) of the peaks on the X-ray diffraction patterns of the products of chemical (**XVI**) and electrochemical (**XVII**, **XVIII**) Mg^{2+} insertion in the hydrated sodium vanadium bronze (**X**).

XVI		XVII		XVIII	
2Θ	I	2Θ	I	2Θ	I
12.38	100	12.68	22	12.11	78
				12.33	65
		18.11	100*	18.10	100*
25.18	45	25.59	47	25.83	74
27.76	55	28.33	30	28.32	59
				38.51	34
				40.33	31
49.27	51	50.28	21	50.65	59

* Peak 100 of triclinic PTFE [23] (from teflonised carbon).

100°C, and a new structure is formed which is able to accommodate significantly less Mg^{2+} than the bronze $NaV_3O_8(H_2O)_{1.5}$. Infrared spectroscopic investigations [4] have shown that water is expulsed, and dehydrated NaV_3O_8 is formed during the drying above 100°C.

3.2. Products of chemical (XVI) and electrochemical (XVII, XVIII) insertion of Mg^{2+} in the partially dehydrated sodium vanadium bronze X

The patterns of the poorly crystalline products **XVI**–**XVIII** of Mg^{2+} insertion in **X** (Fig. 4, Table 3) can also be described using the four basic peaks, as the patterns of **III** and the drying products of **III** discussed above, and can be indexed with the unit cell of barnesite. A layered crystal structure can be proposed for the samples **XVI**–**XVIII**. The size of the unit cell (**Xa**: 344 Å^3, **Xb**: 293 Å^3) decreases during both the chemical (**XVI**: 242 Å^3) and the electrochemical Mg^{2+} insertion (**XVII**: 227 Å^3 and **XVIII**: 262 Å^3). The electrochemically reduced product **XVII** has the smallest value of the unit cell volume. Note that recent electrochemical experiments [4] have shown that a significant amount of Mg^{2+} ions inserted in $NaV_3O_8(H_2O)_y$ during the first voltammetric cycle is irreversibly bonded in the crystal lattice of the bronze. Therefore, the electrochemically cycled, oxidised sample **XVIII** contained trapped Mg^{2+} ions.

The contraction of the unit cell volume of $NaV_3O_8(H_2O)_y$ during Mg^{2+} insertion is not surprising; a similar effect was already observed for cation-intercalated $V_2O_5(H_2O)_{1.6}$ xerogels [24]. The electrostriction phenomenon can explain this behaviour: the intensity of the electrical field surrounding the cation leads to a decrease of the water molecule volume [24].

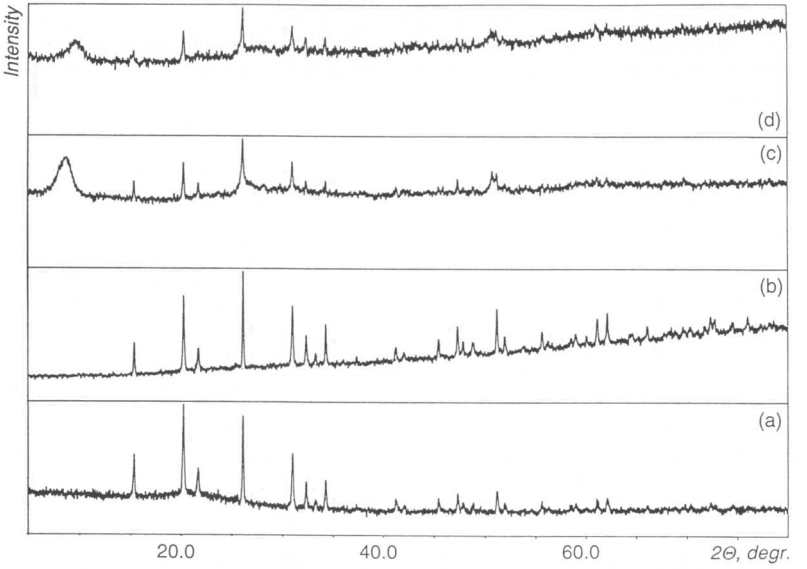

Fig. 5. X-ray powder diffraction patterns of (a) V_2O_5 (**I**), (b) $Mg_xV_2O_5$ (**V**), (c) the bronze $Mg(V_3O_8)_2(H_2O)_y$ dried at 100°C (**XII**), and (d) the product $Mg_{1+x}(V_3O_8)_2(H_2O)_y$ (**XIX**) of chemical Mg^{2+} insertion in **XII**.

The Mg and Na contents, found by EPMA for different microparticles in the product **XVI** of chemical Mg^{2+} insertion in **X**, varied in narrow intervals of 11.7 – 12.2 at.% for Mg, and of 5.4 – 5.8 at.% for Na.

3.3. Products V and XIX of chemical Mg^{2+} insertion in V_2O_5 (I) and in the Mg bronze IV, XII

The X-ray diffractograms of the samples **I**, **V**, **XII** and **XIX** are compared in Fig. 5; the positions of the diffraction peaks are given in Table 4. The patterns of the crystalline sample **I**, and of the product **V** of the chemical Mg^{2+} insertion in **I** are very similar and represent V_2O_5. The V_2O_5 unit cell parameters calculated for **I** and **V**, as well as for those peaks of **XII** and **XIX**, which can be indexed with the V_2O_5 unit cell, are compared in Table 5 with the lattice parameters of electrochemically prepared $Mg_{0.2}V_2O_5$ [10], and of MgV_2O_5 synthesised at 900°C [25]. In contrast to $Mg_{0.2}V_2O_5$, the distribution of peak intensities in **V** is very similar to those observed in **I**, and could indicate an essentially smaller amount of inserted Mg^{2+} in **V** as compared to $Mg_{0.2}V_2O_5$. Indeed, the EPMA investigation showed a content of 1.0 – 1.2 at.% of Mg in sample **V**. (This is in agreement with the conclusion suggested in [3] that water molecules are essential for the Mg^{2+} insertion reaction of V_2O_5. Note that a dry environment is used for the chemical insertion of Mg^{2+} in the present work.)

Table 4. Positions (2Θ, degree) and intensities (I) of the peaks on the X-ray diffraction patterns of the products **V** and **XIX** of chemical Mg^{2+} insertion in V_2O_5 (**I**) and Mg bronze (**XII**).

I		**V**			**XII**			**XIX**			
2Θ	I	$2\Theta_{obs}$	$2\Theta_{calc}$	I	$2\Theta_{obs}$	$2\Theta_{calc}$	I	$2\Theta_{obs}$	$2\Theta_{calc}$	I	hkl
					8.77		65	9.70		39	*
15.34	48	15.37	15.38	36	15.37	15.39	44	15.37	15.39	35	200
20.25	96	20.29	20.28	79	20.29	20.30	79	20.30	20.29	66	001
21.70	29	21.74	21.71	25	21.75	21.73	29				101
26.12	100	26.15	26.15	100	26.16	26.17	100	26.15	26.13	100	110
31.02	62	31.03	31.04	64	31.03	31.06	55	31.01	31.06	62	400
32.34	33	32.38	32.37	33	32.38	32.40	19	32.36	32.36	39	011
34.28	35	34.31	34.31	44	34.33	34.34	28	34.30	34.30	41	310
41.20	17	41.28	41.24	20							002
45.44	17	45.49	45.46	23							411
47.30	22	47.32	47.33	33	47.36	47.36	28				600
					50.78		41	50.68		33	
51.17	26	51.23	51.22	49	51.26	51.26	35	51.16	51.16	35	020
55.61	14	55.63	55.64	21							021
61.05	16	61.13	61.11	29	60.98	61.15	36				321
62.05	16	62.11	62.09	33	62.13	62.13	31				710

* This reflection is contrary to the others, very broad and, thus, assigned to another phase.

Table 5. Unit cell parameters of V_2O_5 (**I**), V_2O_5-related components of **V**, **XII** and **XIX**, and vanadium pentoxide bronzes $Mg_{0.2}V_2O_5$ [10] and MgV_2O_5 [25].

	I	**V**	**XII**	**XIX**	$Mg_{0.2}V_2O_5$	MgV_2O_5
a (Å)	11.5204(9)	11.513(2)	11.508(1)	11.508(8)	11.42	11.019
b (Å)	3.5674(5)	3.5640(6)	3.5617(3)	3.5679(6)	3.552	3.696
c (Å)	4.3780(4)	4.3745(8)	4.370(2)	4.372(2)	4.468	9.965
V (Å^3)	179.93	179.50	179.12	179.50	181.2	405.8

In sample **XII**, the EPMA study showed the presence of microparticles with distinctly different Mg^{2+} content, *viz.* yellow microcrystals with 0.14 at.% of Mg, and brown microcrystals with 1.3–1.5 at.% of Mg. The microparticles of the product **XIX** of the subsequent chemical insertion of Mg in **XII** contain 3.8–4.0 at.% of Mg. Note that several phases related to V_2O_5, and a coexistence of different phases having the same Li content (multiphase domains) were reported for $Li_xV_2O_5$ bronzes [19].

X-ray powder diffraction patterns of the poorly crystalline samples **XII** and **XIX** essentially differ from the patterns of **I** and **V**. Some peaks on the patterns of **XII** and **XIX**, which are present also in **I** and **V**, are broadened

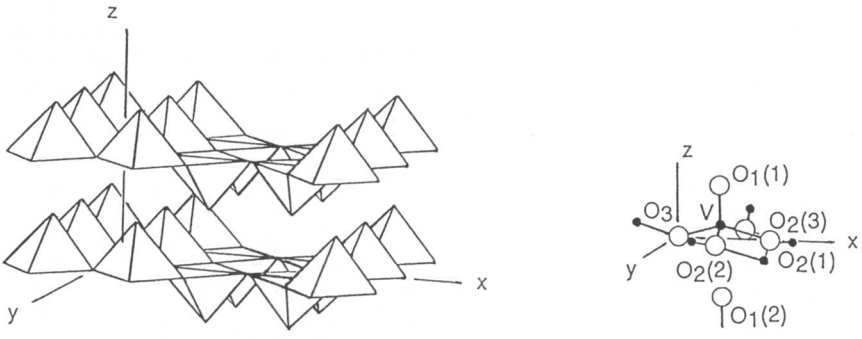

Fig. 6. Crystal structure of V_2O_5 [26].

in comparison with **I** and **V**, but there are also some "new" peaks: (i) Strong and diffuse peaks at $2\Theta = 8.77°$ (**XII**) and 9.70° (**XIX**) which cannot be indexed with the unit cell of **I** or **V** (the first reflection 100, which is actually absent in the measured pattern of **I**, has $2\Theta = 7.67°$); and (ii) new sharp peaks at $2\Theta = 50.78°$ (**XII**) and 50.68° (**XIX**) which are only slightly shifted from the V_2O_5 020 peak at $2\Theta = 51.23°$ in the pattern of **V**. Moreover, there is a hint of a small contraction of the *a* separation of the V_2O_5 crystalline component in the series **I** → **V** → **XII** → **XIX**. A slight shortening of the *a* separation and a slight increase of the *c* separation (corresponding to the interlayer separation in the structure of V_2O_5 [26], Fig. 6) is characteristic for a topotactic insertion in V_2O_5, see, e.g., the structural study of electrochemically formed $Mg_{0.2}V_2O_5$ bronze [10].

Besides the phase with the V_2O_5 structure, we believe that in the new phase(s) of the samples **XII** and **XIX**, a good ordering exists only in one direction, *b'*. The length of this axis is slightly increased in comparison with the *b* separation in **I** and **V**. The value of *b'* is 3.59 Å in **XII**, and 3.60 Å in **XIX** (calculated under an assumption that the new sharp peak in patterns of **XII** and **XIX** is a 020 peak). The new phase(s) of **XII** and **XIX** are disordered in two other directions (i.e. in the *a'c'* planes). Note that an earlier X-ray powder diffraction study of electroformed $Li_xV_2O_5$ bronzes showed a conservation of the *b* separation of the V_2O_5 structure with an increased Li content parallel to more pronounced changes of the *a* and *c* separations [27].

3.4. Products XIII – XV of electrochemical cycling of the V_2O_5 electrode VI

A cyclic voltammogram of the V_2O_5/TC electrode **VI** in an acetonitrile-based electrolyte is shown in Fig. 1. The X-ray diffraction patterns of the electrochemically cycled electrodes **XIII** – **XV** are compared with the pattern of a new electrode **VI** in Fig. 7 and in Table 6. The patterns of the new electrode **VI** and of the oxidised electrode **XV** are very close, and

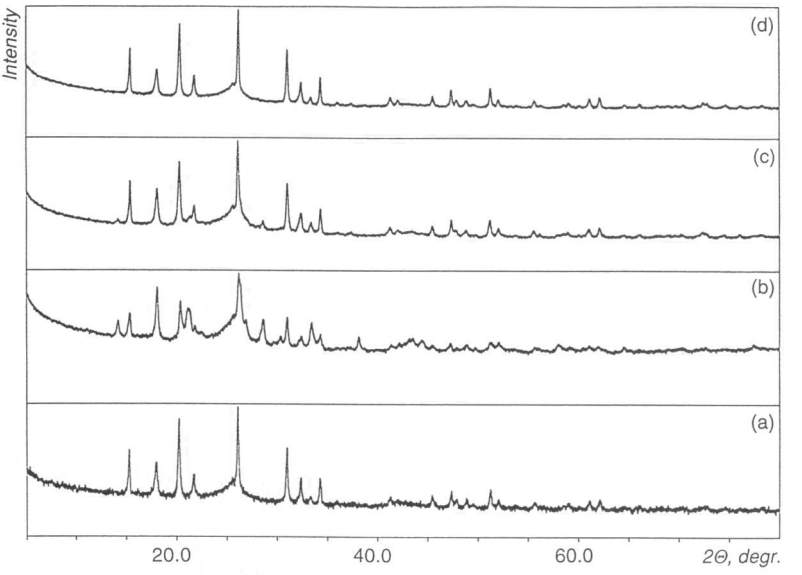

Fig. 7. X-ray powder diffraction patterns of (a) the electrode mass V_2O_5/TC (**VI**) and of the products of electrochemical Mg^{2+} insertion: (b) **XIII** (reduced electrode, after $2^1/_2$ cycles), (c) **XIV** (reduced electrode, after $20^1/_2$ cycles), and (d) **XV** (oxidised electrode, after 20 cycles).

represent a superposition of the pattern of V_2O_5 (or components with the unit cell close to V_2O_5, Table 7), and the mixture of crystalline PTFE and carbon black. The electrochemical reduction of the electrode **VI** leads to the appearance of some "new" peaks in the patterns of **XIII** and **XIV** (besides of the peaks of the V_2O_5 and TC components).

It can be speculated that the appearance of the V_2O_5 features in the reduced electrode means that a fraction of the V_2O_5 is not accessible for the electrochemical reduction. The reason might be a poor electrical contact of V_2O_5 particles to the current collector. This hypothesis is consistent with the fact that in the spring-loaded cell, where the working electrode is mechanically pressed against the current collector, significantly higher coulombic capacities (up to 230 Ah/kg V_2O_5) were reached in comparison with the free-hanging electrodes (about 170 Ah/kg V_2O_5).

But essentially different distribution of the peak intensities of the V_2O_5 component in sample **XIII**, in contrast to the distribution observed for the V_2O_5-containing new electrode **VI**, might indicate the chemical composition $Mg_xV_2O_5$ of this component. The presence of Mg^{2+} in the V_2O_5 microcrystals found in the reduced electrode **XIII** was confirmed by EDX analysis. There is no pronounced change of the unit cell parameters of the V_2O_5 component during the transition from **VI** to **XIII** (Table 7). This

Table 6. Positions (2Θ, degree) and intensities (I) of the peaks on the X-ray diffraction patterns of the products **XIII**–**XV** of electrochemical cycling of the V_2O_5-containing electrode mass **VI**.

VI		**XIII***			**XIV***			**XV***			
2Θ	I	$2\Theta_{obs}$	$2\Theta_{calc}$	I	$2\Theta_{obs}$	$2\Theta_{calc}$	I	$2\Theta_{obs}$	$2\Theta_{calc}$	I	*hkl*
		14.25		22	14.23		5				
15.33	53	15.42	15.37	38	15.45	15.40	52	15.46	15.41	54	200
18.02	79**	18.17		79**	18.16		43**	18.17		31**	
20.26	91	20.39	20.36	63	20.35	20.34	75	20.38	20.35	82	001
		21.10		56							
		21.35		41	21.36		8				
21.70	28	21.81	21.79	23	21.79	21.77	20	21.81	21.78	25	101
		22.03		13							
		22.49		12							
25.79	16	25.87	25.61	34	25.68	25.61	21	25.94	25.62	16	201
26.12	100	26.22	26.20	100	26.21	26.18	100	26.24	26.23	100	110
		27.01		34							
		28.40		20							
		28.65		34	28.67		11				
		30.36		13							
31.02	65	31.06	31.02	48	31.12	31.04	60	31.12	31.05	62	400
32.39	29	32.44	32.47	18	32.43	32.42	26	32.48	32.48	26	011
		33.48	33.41	37	33.44	33.37	16				111
34.27	31	34.39	34.34	22	34.38	34.35	33	34.40	34.40	32	310
		38.18		23							
41.33	11	41.44	41.41	11	41.33	41.35	12	41.36	41.37	12	002
		43.54		17	43.56		8				
		43.76		12							
		44.44		17	44.43		5				
45.42	13	45.46	45.52	10	45.50	45.54	13	45.57	45.59	13	411
47.40	20	47.29		12	47.42		22	47.44		20	600
47.93	11	47.95	47.97	11	47.91	47.94	10				302
48.98	10	49.00	48.99	15							012
51.27	22	51.35	51.34	18	51.28	51.27	22	51.31	51.39	22	002
52.09	13	52.14	52.00	19	52.10	52.09	13				601
		58.05		18							
59.10	11										412
61.11	12				61.19	61.18	11	61.21	61.27	11	321
62.17	14				62.19	62.20	13	62.20	62.26	13	710

* See the discussion of not indexed reflections in the text.
** Peak of PTFE (from teflonised carbon).

indicates that V_2O_5 can be regarded as a three-dimensional framework host, rather than a two-dimensional one (as already suggested in studies of Li^+ insertion in V_2O_5 [20, 28]).

Table 7. Unit cell parameters of V_2O_5-related components of the electrode mass **VI** and the products **XIII – XV** of its electrochemical cycling.

	VI	XIII	XIV	XV
a (Å)	11.533(6)	11.520(7)	11.495(3)	11.489(3)
b (Å)	3.562(1)	3.556(2)	3.561(1)	3.553(1)
c (Å)	4.376(4)	4.357(2)	4.363(2)	4.3609(9)
V (Å^3)	179.93	178.50	178.62	178.02

The unit cell parameters of chemically (**V**) and electrochemically (**XIII**) formed $Mg_xV_2O_5$ are very close (cf. Tables 5 and 7). Thus, the products of Mg^{2+} insertion in V_2O_5 might be similar in both cases.

The new peaks appearing in the X-ray diffractogram of the V_2O_5/TC electrode reduced at -1.4 V (vs. Ag/Ag^+) after $2^1/_2$ voltammetric cycles (**XIII**) can be separated into two groups: (i) five peaks present also in the sample **XIV** reduced after $20^1/_2$ voltammetric cycles, and (ii) peaks present only in **XIII** (Table 6). These two groups of peaks have to belong to different phases (e.g. **XIIIa** and **XIIIb**), because, e.g., the strongest new peak in the pattern of **XIII** (at $2\Theta = 21.10°$) is absent in the pattern of **XIV**. Thus, the reduced electrode **XIII** may consist of five phases: V_2O_5 (or $Mg_xV_2O_5$), carbon black, PTFE, **XIIIa** (which exists also in **XIV**), and **XIIIb**.

The amount of the phase **XIIIb** in the electrode obviously decreases during cycling as evidenced by the absence of corresponding peaks in the diffractogram of the electrode **XIV** reduced after $20^1/_2$ cycles. This behaviour is consistent with the known fact that $Mg_xV_2O_5$ exists in two phases – a stable orthorhombic α phase ($0 < x < 0.11$) and a metastable ζ phase [6]. Note the **XIIIa** and **XIIIb** phases are absent in the oxidised, cycled electrode **XV**, so they are products of reversible V_2O_5 reduction. The indexing of the **XIIIb** phase is ambiguous. One of the solutions is an orthorhombic unit cell [$a = 17.69(1)$ Å, $b = 13.003(4)$ Å, $c = 3.360(2)$ Å, $V = 773$ Å^3] with one period equal to that observed in MgV_2O_5 and the unit cell volume four time larger as of MgV_2O_5. Also the unit cell of the phase **XIIIa** cannot be elucidated, because the indexing of the corresponding lines gives several solutions of comparable reliability. Thus, the electrochemical reduction of **VI** seems to lead to both (i) Mg^{2+} insertion in V_2O_5 with the conservation of the V_2O_5 structure, and (ii) formation of new Mg,V-containig phase(s) (**XIIIa** or **XIIIa + XIIIb**).

The TEM study of **XIII** confirmed the presence of microcrystals with the unit cell close to V_2O_5 in electrochemically reduced samples. There were obtained, besides the common V_2O_5 diffraction, two kinds of diffraction patterns. The interplanar distances from the first one are $d_1 = 9.7$ Å and $d_2 = 25.0$ Å. The patterns of the second kind indicate a superstructure (Fig. 8). All the microcrystals are very thin plates oriented normal to the

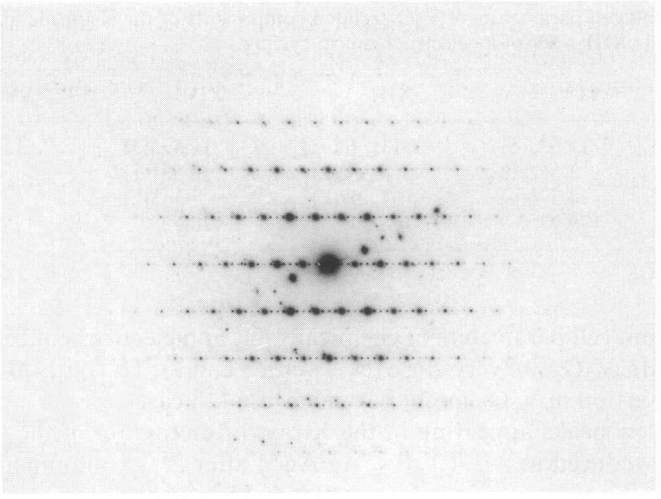

Fig. 8. Diffraction pattern of a microcrystal of the reduced electrode **XIII**.

beam direction; recording of diffraction patterns suitable for the determination of the interplanar distance for the "third direction" was therefore not possible. We did not succeed in performing a reliable analysis confirming the presence of Mg within the grains exhibiting the superstructure.

The electrode **XIV** consists of four phases: one with the unit cell of V_2O_5, carbon black, PTFE, and a new phase structurally related to V_2O_5. The change of the structure of the products of electrochemical cycling with the number of cycles (note the observed difference between the electrodes **XIII** and **XIV**) was discussed also in [19] for electrochemically inserted $Li_xV_2O_5$.

3.5. Electrochemical Mg^{2+} insertion in the V_2O_5 single crystal II

The V_2O_5 single crystals (**II**) lost the single crystallinity after the electrochemical Mg^{2+} insertion. An optical micrograph of the crystal **VIII** showed broad lines and shadows of the dark $Mg_xV_2O_5$ within the orange-yellow V_2O_5 crystal. Obviously, the insertion process is very nonuniform. The EDX analysis did not indicate the presence of Mg. Thus, the amount of Mg^{2+} inserted in the single crystals was rather low. The chemical insertion of Mg^{2+} in the V_2O_5 single crystal resulted in no apparent colour change.

4. Conclusions

The chemical and the electrochemical Mg^{2+} insertion in V_2O_5 seems to produce similar V_2O_5-related phases. But the electrochemical reduction of

V_2O_5 in PTFE-bonded electrodes is more complex and rather nonuniform. At least two new phases (both possibly $Mg_xV_2O_5$ phases) are formed during the reversible reduction of V_2O_5 in wet acetonitrile containing $Mg(ClO_4)_2$. The presence of one of the new phases in the electrode decreases during electrochemical cycling. Upon reoxidation, the original V_2O_5 structure of the $Mg_xV_2O_5$ phases appears to be restored. In the hydrated sodium vanadium bronzes, $NaV_3O_8(H_2O)_y$, two layered phases with different water content coexist. The phase $NaV_3O_8(H_2O)_{1.5}$ is electrochemically the most active one, which allows Mg^{2+} insertion from rigorously dry electrolytes. Dehydration occurring above 100° C causes a decrease of the interlayer separations as well as a decrease in the coulombic capacity of the bronze, so the preparation and drying of the bronzes below 100° C is recommended.

Acknowledgements

We thank Dr. O. Haas, PSI, for many stimulating discussions. We are also indebted to Dr. K. Kato of the National Institute of Inorganic Materials, Tsukuba, Japan, for the donation of the V_2O_5 single crystals, R. Wessicken, ETH, for STEM measurements, H. Meyer zu Altenschildesche, ETH, for NMR measurements, F. Ried, ETH, for EPMA study, and W. Scheifele, PSI, for technical assistance. This work was supported by the Swiss "Bundesamt für Energiewirtschaft" (Grant No. EF-PROCC(91)018).

References

1. T. D. Gregory, R. J. Hoffman and R. C. Winterton, J. Electrochem. Soc. **137** (1990) 775.
2. R. J. Hoffman, R. C. Winterton and T. D. Gregory, US Pat. 4,894,302 (1990).
3. P. Novák and J. Desilvestro, J. Electrochem. Soc. **140** (1993) 140.
4. P. Novák, W. Scheifele and O. Haas, Molten Salt Forum **1–2** (1993/94) 389.
5. J. Galy and M. Pouchard, Bull. Soc. Chim. France (1967) 261.
6. J. Galy, M. Pouchard, A. Casalot and P. Hagenmuller, Bull. Soc. Fr. Mineral. Cristallogr. **90** (1967) 544.
7. R. Schöllhorn and H. Meyer, Mat. Res. Bull. **9** (1974) 1237.
8. R. Schöllhorn and W. Schmucker, Z. Naturforsch. **30b** (1975) 975.
9. A. Lerf and R. Schöllhorn, Inorg. Chem. **16** (1977) 2950.
10. J. P. Pereira-Ramos, R. Messina and J. Perichon, J. Electroanal. Chem. **218** (1987) 241.
11. P. G. Bruce, F. Krok, J. Nowinski, V. C. Gibson and K. Tavakkoli, J. Mater. Chem. **1** (1991) 705.
12. P. Lightfoot, F. Krok, J. L. Nowinski and P. G. Bruce, J. Mater. Chem. **2** (1992) 139.
13. P. G. Bruce, F. Krok, P. Lightfoot, J. L. Nowinski and V. C. Gibson, Solid State Ionics **53–56** (1992) 351.
14. R. E. Dueber, J. M. Fleetwood and P. G. Dickens, Solid State Ionics **50** (1992) 329.
15. F. Joho, P. Novák, O. Haas and R. Nesper, Chimia **47** (1993) 288.

16. K. Kato, personal communication, June 1992.
17. R. Gutmann, J. Hulliger and E. Reusser, J. Cryst. Growth **126** (1993) 578.
18. A. D. Weeks, D. R. Ross and R. F. Marvin, Am. Mineral. **48** (1963) 1187.
19. J. M. Cocciantelli, J. P. Doumerc, M. Pouchard, M. Broussely and J. Labat, J. Power Sources **34** (1991) 103.
20. J. A. Jacobson: "Intercalation Reactions of Layered Compounds", in *Solid State Chemistry. Compounds* (A. K. Cheetham and P. Day, Eds.), p. 217. Clarendon Press, Oxford, (1992).
21. K. Kato and E. Takayama, Acta Crystallogr. **B40** (1984) 102.
22. O. P. Lapina, V. M. Mastikhin, A. A. Shubin, V. N. Krasilnikov and K. I. Zamaraev, Prog. Nucl. Magn. Reson. Spectrosc. **24** (1992) 457.
23. H. G. Killian, Kolloid-Z. **185** (1962) 13.
24. N. Baffier, L. Znaidi and J.-C. Badot, J. Chem. Soc. Faraday Trans. **86** (1990) 2623.
25. J. C. Bouloux, I. Milosevic and J. Galy, J. Solid State Chem. **16** (1976) 393.
26. H. G. Bachmann, F. R. Ahmed and W. H. Barnes, Z. Kristallogr. **115** (1961) 110.
27. S. Hub, A. Tranchant and R. Messina, Electrochim. Acta **33** (1988) 997.
28. D. W. Murphy, P. A. Christian, F. J. DiSalvo and J. V. Waszczak, Inorg. Chem. **18** (1979) 2800.